

Soft Matter

Accepted Manuscript



This is an *Accepted Manuscript*, which has been through the Royal Society of Chemistry peer review process and has been accepted for publication.

Accepted Manuscripts are published online shortly after acceptance, before technical editing, formatting and proof reading. Using this free service, authors can make their results available to the community, in citable form, before we publish the edited article. We will replace this *Accepted Manuscript* with the edited and formatted *Advance Article* as soon as it is available.

You can find more information about *Accepted Manuscripts* in the [Information for Authors](#).

Please note that technical editing may introduce minor changes to the text and/or graphics, which may alter content. The journal's standard [Terms & Conditions](#) and the [Ethical guidelines](#) still apply. In no event shall the Royal Society of Chemistry be held responsible for any errors or omissions in this *Accepted Manuscript* or any consequences arising from the use of any information it contains.

Pathways of Cylindrical Orientations in PS-*b*-P4VP Diblock Copolymer Thin Films upon Solvent Vapor Annealing

E. Bhoje Gowd^{1,2,3*}, Tadanori Koga², Maya K. Endoh,² Kamlesh Kumar³ and Manfred Stamm^{3,4}

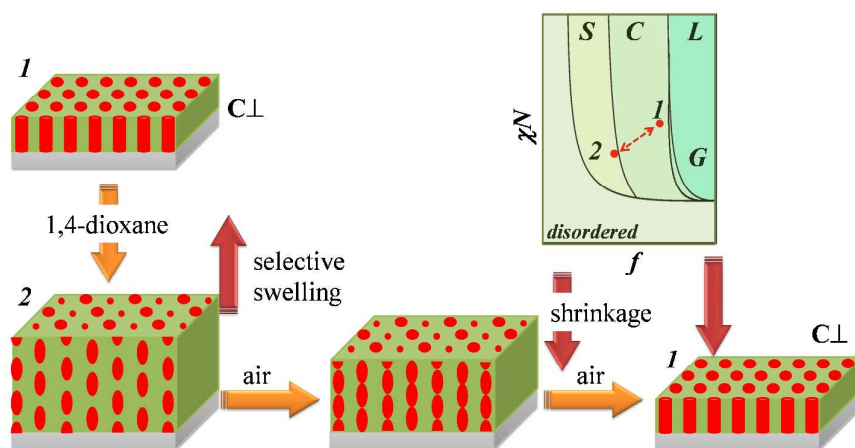
¹Materials Science and Technology Division, CSIR-National Institute for Interdisciplinary Science and Technology, Trivandrum-695 019, Kerala, India

²Chemical and Molecular Engineering Program, Department of Materials Science and Engineering, Stony Brook University, Stony Brook, NY 11794-2275, USA

³Department of Nanostructured Materials, Leibniz Institute of Polymer Research Dresden, Hohe Strasse 6, 01069, Dresden, Germany

⁴Physical Chemistry of Polymer Materials, Technische Universität Dresden, 01062 Dresden, Germany

FOR TABLE OF CONTENTS ONLY



Pathways that control the orientations of cylindrical microdomains formed in PS-*b*-P4VP thin films upon annealing in different solvent vapors were clarified using time-resolved in situ GISAXS and ex-situ scanning force microscopy.

Pathways of Cylindrical Orientations in PS-*b*-P4VP Diblock Copolymer Thin Films upon Solvent Vapor Annealing

E. Bhoje Gowd^{1,2,3*}, Tadanori Koga², Maya K. Endoh,² Kamlesh Kumar³ and Manfred Stamm^{3,4}

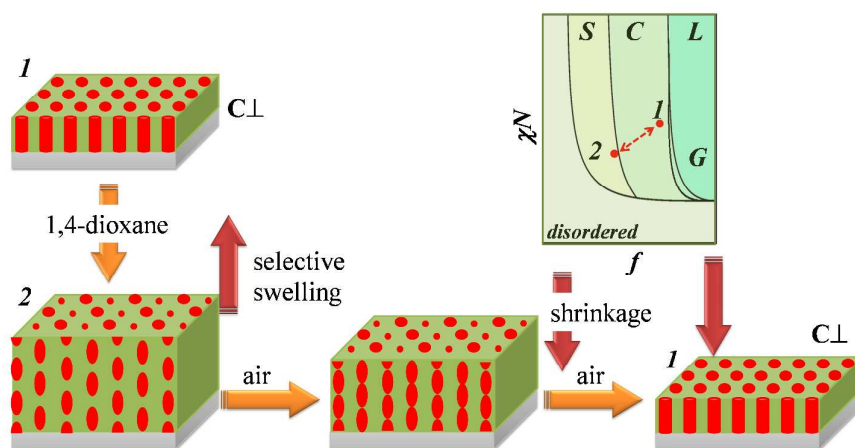
¹Materials Science and Technology Division, CSIR-National Institute for Interdisciplinary Science and Technology, Trivandrum-695 019, Kerala, India

²Chemical and Molecular Engineering Program, Department of Materials Science and Engineering, Stony Brook University, Stony Brook, NY 11794-2275, USA

³Department of Nanostructured Materials, Leibniz Institute of Polymer Research Dresden, Hohe Strasse 6, 01069, Dresden, Germany

⁴Physical Chemistry of Polymer Materials, Technische Universität Dresden, 01062 Dresden, Germany

FOR TABLE OF CONTENTS ONLY



* Corresponding author.

E-mail: bhojegowd@niist.res.in

Tel: +91 471 2515474, Fax: +91 471 2491712

Abstract

The orientation changes of perpendicular cylindrical microdomains in polystyrene-*block*-poly(4-vinylpyridine) (PS-*b*-P4VP) thin films upon annealing in different solvent vapors were investigated by in situ grazing incidence small-angle X-ray scattering (GISAXS) and ex-situ scanning force microscopy (SFM). The swelling of the P4VP perpendicular cylinders ($C\perp$) in chloroform, a non-selective solvent vapor leads to the reorientation to in-plane cylinders through a disordered state in a particular kinetic pathway in the phase diagram upon drying. On the other hand, the swelling of the P4VP perpendicular cylinders in a selective solvent vapor (i.e., 1,4-dioxane) induces a morphological transition from cylindrical to ellipsoidal as a transient structure to spherical microdomains; subsequent solvent evaporation resulted in shrinkage of the matrix in the vertical direction, merging the ellipsoidal domains into the perpendicularly aligned cylinders. In this paper, we discussed the mechanism based on the selectivity of the solvent to the constituting blocks that is mainly responsible for the orientation changes.

Introduction

Block copolymers consisting of chemically dissimilar blocks usually self-assemble into microphase-separated domains below the order-disorder transition temperature.¹⁻⁴ This is a thermodynamically driven process that leads to periodic nanoscale structures with length scales ranging from 10 to 100 nanometres. The formation of the microdomain structures in bulk has been extensively studied from both theoretical and experimental points of view and explained by taking into account of interaction energies of blocks, block chain ratios and variations in entropy as a function of chain lengths.¹⁻⁸ Monolayer films of block copolymers have recently received significant attention because of their potential nanofabrication applications, such as nanostructured membranes,^{9,10} nanoparticle templates,¹¹⁻¹⁴ photovoltaic

cells,¹⁵ low- k dielectrics,¹⁶ and high density data storage media.¹⁷ For most of these applications, long-range lateral order and the orientation of the microdomains are of great importance.

In the case of block copolymer thin films, however, film thickness and two types of interfacial interactions (i.e., block copolymer-air surface and block copolymer-substrate interactions) play a crucial role in controlling the orientation and ordering of microdomain structures.¹⁸⁻²⁰ A number of strategies including the use of external forces such as electric field,^{11,21-23} shear force,²⁴ chemically patterned substrates,^{25,26} directional solidification,^{27,28} supramolecular assembly with small molecules,^{29,30} thermal annealing above glass transition temperatures of both blocks³¹⁻³³ and solvent vapor annealing³⁴⁻⁴⁵ have been developed to control the orientation and to prepare highly ordered block copolymer thin films on substrates. Among these methods, solvent vapor annealing is a simple and effective method to manipulate the orientation of block copolymer microdomains in thin films.³⁴⁻⁴⁵ Interested readers are referred to recent perspective on solvent vapor annealing of block copolymer thin films reported by Sinturel et al.⁴⁴ It is known that the microdomain orientation and long-range order are controlled by parameters of solvent vapor annealing including swelling ratios, a time in the equilibrated swollen state and deswelling rates of block copolymer thin films. These parameters are dictated by a solvent used for solvent vapor annealing process, i.e., selectivity of the solvent to one of the blocks, vapor pressure and boiling point of the solvent.⁴⁴ Most of previous studies on solvent vapor annealing of block copolymer thin films have been done based on surface probing techniques such as scanning force microscopy, scanning electron microscopy or transmission electron microscopy. These techniques give us information about the local structures at the top surface, but it is difficult to reveal the inner structures. Although a cross section of a film allows for probing the interior structures, a lack

of contrast often prevents direct imaging without staining. Furthermore these real space techniques are limited to only the dried state (pre or post annealed samples).

Considering the importance of a monolayer block copolymer thin film covering on a substrate in nanofabrication, it is necessary to understand their interior microdomain structures during switching between different alignments.^{13,14,42} Moreover, in order to address a challenge of improving the long range order of microdomains, it is crucial to understand the structural changes during solvent vapor annealing. Grazing-incidence small-angle X-ray scattering (GISAXS) is a powerful tool to assess interior morphologies of thin films quantitatively in the swollen state.^{38,40,41,43,46,47} Particularly in situ real time GISAXS measurements during solvent annealing (i.e., swelling and deswelling) are quite useful to understand pathways of orientational changes in microdomain structures of block copolymer thin films. For example, Ober and co-workers demonstrated that cylinder-sphere phase transition occurs upon selective solvent vapor annealing of a poly(α -methylstyrene)-*b*-poly(4-hydroxy styrene) thin film. In this system, the structure in the swollen state was kinetically trapped in the dry state due to fast evaporation of the solvent.⁴⁷ In another study, Paik et al. monitored the real time structural changes occurring in thin films of poly(α -methylstyrene)-*b*-poly(4-hydroxy styrene) in the swollen state using vapors of selective (acetone) and non-selective solvent (tetrahydrofuran (THF)) using GISAXS.⁴⁸ It was demonstrated that the plasticization effect of the solvent vapors (chain mobility) controls the structural reorganizations. Swelling the film containing perpendicularly oriented cylinders with a non-selective solvent (THF) induced the orientation change to parallel cylinders in the dried state, while in the case of a selective solvent (acetone), an order-order transition (cylinder-sphere) occurs instead.⁴⁸ In a previous paper, we also reported the cylinder-sphere phase transition upon selective solvent vapor annealing of a polystyrene-*block*-poly(4-vinylpyridine) (PS-*b*-P4VP) thin film.⁴¹ These in situ scattering studies suggest that if the chosen solvent is

selective to one of the blocks, the selective swelling of one of constituent blocks induces an order-order transition and the final microdomain structure depends upon the evaporation rate of the solvent.^{41,48} However, the detailed mechanism remains unclear yet, since it is believed to be a kinetic phenomenon largely determined by preparations procedures.

In this study, we aim to understand the mechanism of orientational changes of cylindrical microdomains formed in PS-*b*-P4VP thin films annealing with both nonselective (chloroform) and selective solvent vapors (1,4-dioxane) by using a combination of in situ GISAXS and ex-situ SFM. PS-*b*-P4VP is a widely studied block copolymer system for self-assembly and nanofabrication as it possess a high Flory-Huggins interaction parameter at room temperature.^{49,50} Furthermore, it is widely used for the formation of supramolecular thin films, since P4VP can be used effectively for the formation of hydrogen bonding with small molecules.^{13,29,30} The solubility parameters of chloroform, 1,4-dioxane, PS, and P4VP blocks are reported to be 19.0, 20.5, 18.6, and 22.2 MPa^{1/2}, respectively. Here we show that the selectivity of solvent vapor to the block chains results in different pathways and final structures of P4VP cylindrical microdomain; (i) the use of chloroform, a non-selective solvent vapors, leads to the reorientation from perpendicular cylinders to in-plane cylinders via a disordered state; (ii) 1,4-dioxane, which is preferential solvation for PS chains, induces a morphological transition from perpendicular cylinders to ellipsoids as a transient structure to spherical microdomains and subsequent solvent evaporation recovers the perpendicularly aligned cylinders. Based on the present experimental data, we propose models upon the solvent vapor annealing of block copolymer thin films with non-selective and selective vapors. We believe that the present results provide a better understanding of essential features of solvent vapors that induce orientations of cylindrical microdomains in diblock copolymer thin film.

Experimental Section

Materials and Thin films preparation: PS-*b*-P4VP with number average molecular masses of $M_n=32900$ g/mol for PS, $M_n=8000$ g/mol for P4VP, $M_w/M_n = 1.06$ for both blocks was purchased from Polymer Source, Inc. PS-*b*-P4VP was dissolved in chloroform, a nonselective solvent, to obtain a 1 wt% polymer solution. The polymer solution was filtered several times through Millipore 0.2 μm Teflon filters. Thin films were then prepared by a dip-coating process at a speed of 1.0 mm s^{-1} onto silicon wafers, which was cleaned with dichloromethane in an ultrasonic bath for 20 min followed by further cleaning in a 1:1:1 mixture of 29% ammonium hydroxide, 30% hydrogen peroxide and water (*Warning: This solution should not be stored in tightly sealed containers as it is extremely corrosive*) for 1.5 h at 65 °C. Single-crystal silicon wafers with a (100) orientation were purchased from Semiconductor Processing Co. The films were further annealed in the vapors of 1,4-dioxane for vertical alignment of the cylindrical microdomains.⁴² Porous templates were obtained by surface reconstruction of thin films in ethanol, a selective solvent for P4VP.

Characterization: The thickness of the polymer films was measured by a SE400 ellipsometer (SENTECH Instruments GmbH, Germany) with a laser (the wavelength of 632.8 nm) at an incident angle of 70°. The thicknesses of all the films coated on silicon substrates were fixed to 28 ± 2 nm. Scanning force microscope (SFM) experiments were performed using a Dimension 3100 scanning force microscope (Digital Instruments, Inc., Santa Barbara) with a tapping mode to understand the film topology and surface morphology. A glass chamber with an air tight cap was used with the volume ($V = 250$ cm^3) and surface area ($S = 27$ cm^2) for ex-situ experiments. Another chamber with kapton windows having same size was designed for in situ GISAXS experiments, where saturation of solvent vapors can be controlled between 0 to 100%. This chamber has inlets for solvent vapors as well as inert gas flow. After swelling the films in saturated vapors for the required time, immediately

nitrogen gas was injected to dry the films where both chloroform and 1,4-dioxane evaporated within a fraction of a second. GISAXS measurements were performed at ID10B beam line (X-ray energy of 8 keV ($\lambda=0.15377$ nm)) at the European Synchrotron Radiation Facility (ESRF), Grenoble, France. The images were captured by a MAR CCD camera with a pixel size of $64.45 \mu\text{m}$ and resolution of 2048×2048 . The sample to detector distance, which was calibrated with silver behenate standard, was 0.39 m. The films were irradiated with the fixed incident angle (α_i) of 0.20° , which is just above the critical angle of PS-*b*-P4VP sample, such that the entire film structures are discussed. The GISAXS measurements started just after the injection of the solvent vapors to the annealing chamber. Data were collected at every 15 s. The 2-dimensional GISAXS patterns were processed using Fit2D free software to convert into 1-dimensional intensity profiles in the q_y - q_z plane, where q_y is the scattering vector parallel to the film surface and q_z is the scattering vector perpendicular to the film surface.

Results and Discussion

Solvent vapor annealing of perpendicular cylinders ($C\perp$) in the nonselective solvent (chloroform):

To explore the pathways of orientation switching from perpendicular to parallel morphology ($C\perp$ to $C//$), after the 1,4-dioxane vapor annealing ex situ SFM experiments were utilized to characterize surface morphologies of the PS-*b*-P4VP thin films. PS-*b*-P4VP thin films annealed in 1,4-dioxane vapor assemble into hexagonally packed cylindrical microdomains oriented normal to the substrate surface ($C\perp$) (Figure 1, $t=0$). To enhance the contrast of the SFM images, the resultant films were further immersed in ethanol, a preferential solvent for P4VP and a non-solvent for PS, to make porous film by reconstructing the surface. This process was called as surface reconstruction.^{42,50,51} Russell and co-workers have shown that such a surface reconstruction process with the use of a selective solvent for PS-*b*-P4VP

diblock copolymer thin films does not alter the order or orientation of the microdomains.^{50,51} We confirmed that surface reconstruction of 1,4-dioxane vapor annealed film persists the well-developed $C\perp$ microdomain structure having hexagonal packing with an average center-to-center spacing of 26 ± 2 nm and pore diameter of 8 ± 1 nm. The corresponding fast Fourier transformation images (shown in the inset) support the formation of the ordered hexagonal packing structures at the film surface. These samples were further annealed in chloroform vapor, which is a nonselective solvent for PS-*b*-P4VP, for different times. Figure 1 shows the SFM height images of the films annealed in chloroform vapors for different times. The scanning force microscope (SFM) images shown in Figure 1 correspond to the stage after the surface reconstruction in ethanol. From the figure we can see that the films annealed in chloroform vapor for 2 and 4 minutes display the identical surface morphology. However, significant changes were observed in the 6 min annealed sample and the resultant surface morphology looks like disordered wormlike morphology. The perpendicular cylindrical microdomains were deformed significantly and almost disappeared. On further increasing the annealing time to 8 min, the orientation is switched to the parallel one. As seen from the figure, the cylinders are not continuous. After 14 min annealing, the cylinders became more continuous and the resultant morphology completely switched to well-ordered parallel cylindrical morphology. These results demonstrated that 8 min chloroform vapor annealing in saturated vapors induces the switching of the orientation to parallel cylindrical morphology. However, the order of the parallel cylinders is poor due to the insufficient mobility of the polymer chains in the swollen state. Further increase in the annealing time accelerates the chain mobility, allowing the structure to reach towards the equilibrium morphology (i.e., parallel cylinders). Although the thickness of the film in the swollen state could not be measured directly, we speculate that it increases with annealing time and plays a crucial role in controlling the microdomain orientation.^{48,52} The surface reconstruction of the films

annealed in chloroform vapors for 14 min showed nanochannels (a center-to-center spacing of $\sim 30 \pm 2$ nm.) oriented parallel to the substrate surface ($C//$) because of preferential solvation of P4VP block.

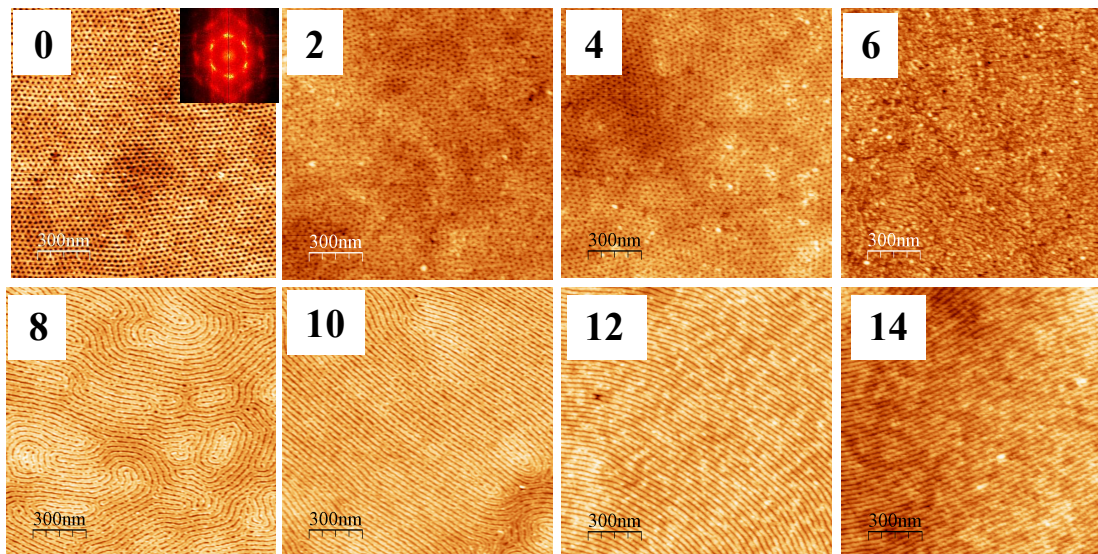


Figure 1. SFM height images of the PS-*b*-P4VP thin film with original perpendicular cylindrical morphology ($C\perp$) at $t=0$ and then annealed in chloroform vapor at different times (all the images are taken after surface reconstruction in ethanol to show the better contrast). The numbers indicated at the left top of the images corresponds to the elapsed times (in minutes) in chloroform vapor.

To assess the morphology in the swollen state and to understand the pathways of the orientational switching from perpendicular cylinders to parallel cylinders, in situ GISAXS experiments were performed. Sequences of GISAXS images are shown in Figure 2 at different intervals of time during chloroform vapor annealing of the $C\perp$ oriented block copolymer thin film. It should be noted that the GISAXS image at $t=0$ min corresponds to the time just after surface reconstruction in ethanol (a good solvent for P4VP, but a non-solvent for PS). The GISAXS image ($t=0$) prominently features sharp Bragg rods (i.e., vertical streaks) up to fourth order and the ratios of the higher order peak positions can be assigned to

2:3:4 relative to the first order peak position. The corresponding SFM image reflects the hexagonally ordered perpendicular cylinders with an average center-to-center spacing of 26 ± 2 nm, which is very close to the periodic spacing calculated from the first maximum of GISAXS Bragg rod (28.8 nm).

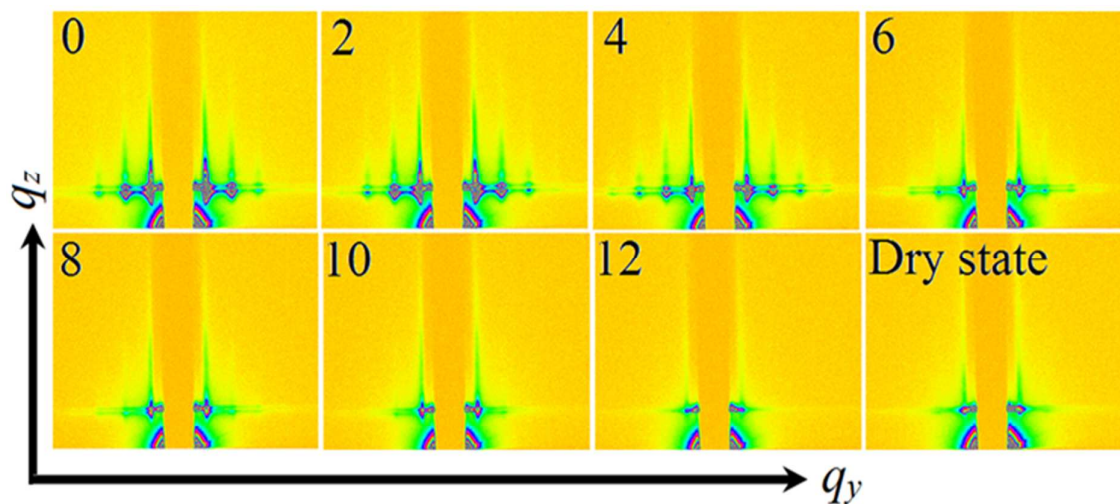


Figure 2. Time-resolved GISAXS images collected for the perpendicularly oriented PS-b-P4VP cylinders (C_{\perp}) upon exposure to saturated chloroform vapors. The last image (indicated by “dry state”) was collected after drying the film. The number on each image represent chloroform vapor exposure time in minutes. Data are from Ref. 41.

There are a few possibilities to explain the appearance of high-order Bragg rods with relative peak positions of 2:3:4 even for hexagonally ordered perpendicular cylinders. The first possibility is that the film has parallel cylindrical microdomains, but this can be ruled out by the fact that the SFM image shows the perpendicular cylinders. Rather, as Russell and co-workers pointed out,¹⁷ it is likely that the grain sizes of the cylindrical microdomains are comparable to the size of the coherence length of X-ray beam ($\sim 1 \mu\text{m}$) such that additional in-plane alignment of the film is required to satisfy the Bragg condition. For example, Bragg rods are seen at scattering vectors characteristic of the $(h,0)$ planes, where h is an integer, of a

hexagonal array of cylindrical microdomains oriented normal to the surface that are truncated at the surface. No evidence of (hk) reflections, where k is nonzero, is observed, indicating the perfect orientation of the lattice over the area exposed to the X-ray beam.^{17,41} In fact, we performed further GISAXS experiments and confirmed an appearance of the $\sqrt{3}$ peak at a specific (in-plane) rotation of the film (Figure S1). In addition, the SFM image supports that the grain size is larger than $1 \mu\text{m}$.

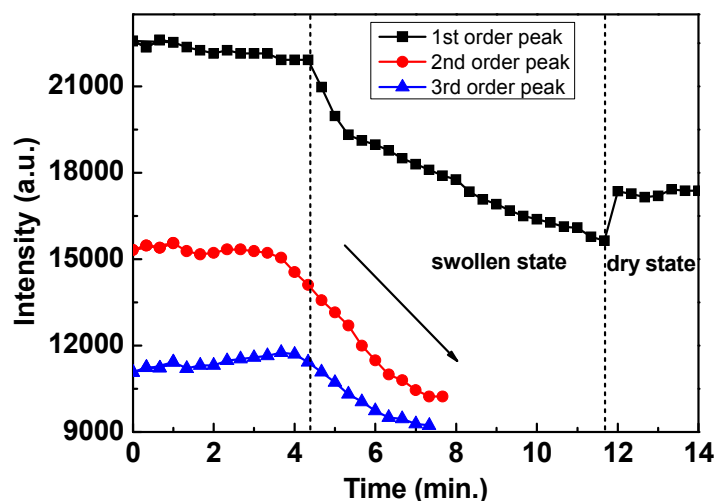


Figure 3. Time-resolved *in-plane* GISAXS intensity maximum of 1st, 2nd and 3rd order scattering peaks evaluated from *in-plane* GISAXS line profiles collected for the perpendicularly oriented PS-*b*-P4VP cylinders ($C\perp$) upon exposure to saturated chloroform vapors.

The variations in the peak intensities of the first, second and third order peaks of the *in-plane* GISAXS (intensity vs q_y) are plotted against the time in Figure 3. Upon exposure to chloroform vapors, the deviation from the linear behavior of the intensity change at $t = 4$ min might be attributed to the onset of order-disorder transition (ODT). The second and higher order peaks completely disappeared when the exposure time reached 8 min., and the intensity of the first order peak also decreases drastically. It is worth mentioning here that such a

drastic change in the intensity of SAXS reflections versus temperature can be seen at the order-disorder transition in bulk block copolymer samples.⁵³⁻⁵⁵ At the same time, *out-of-plane* GISAXS (intensity vs q_z) line profiles did not show any obvious changes in the presence of the solvent vapors. Figure S2 shows the *out-of-plane* GISAXS line profile at $t = 10$ min (swollen state). No evidence of microphase separation between PS and P4VP is observed in the *out-of-plane* GISAXS pattern collected after 10 min (in the swollen state) indicating the miscibility of PS and P4VP chains in the swollen state due to order-disorder transition. After solvent removal (at $t=12$ min) the first order Bragg rod developed again (intensity of the first order peak increases), indicating the structural reorganization. Based on the GISAXS data and SFM data, it is speculated that the solvent facilitates the non-favourable interactions between the segments forcing the cylinders to deform first and then undergo coalescence with the neighbouring deformed cylinders to form the disordered state. We propose the following model to explain the re-orientation from perpendicular cylinders to parallel cylinders upon the solvent vapor annealing.

Figure 4 shows a schematic diagram of the microdomain re-orientation upon swelling in the non-selective solvent (i.e. chloroform) and the effect can be incorporated in the phase diagram χN vs f . Chloroform is expected to be uniformly distributed in the polymer film and impart chain mobility as a plasticizer.⁵⁶ Many previous studies reported the depression of glass transition temperature of block copolymers under solvent vapor uptake.^{43,48,57-59} In addition, absorption of the vapors reduces the effective interaction parameter between the two blocks. Green and co-workers explained the effect of solvent vapors on the phase behavior of block copolymers.⁶⁰ According to their study, the effective interaction parameter (χ_{eff}) between blocks in the presence of low molecular weight component can be approximated to be

$$\chi_{\text{eff}} \approx \phi(\chi_{\text{AB}} + \Delta\chi) = \phi(\chi_{\text{AB}} + \chi_{\text{A-S}} - \chi_{\text{B-S}}) \quad (1)$$

where φ is the volume fraction of a block copolymer in the solvent, and $\Delta\chi$ is the difference between the A-solvent and B-solvent interaction parameters χ_{A-S} and χ_{B-S} . It was assumed that χ_{A-S} and χ_{B-S} are not strongly dependent upon a polymer concentration. In the case of a nonselective solvent, $\Delta\chi \sim 0$ can be reasonably assumed. Hence, uniform swelling of a diblock copolymer in a nonselective solvent vapor leads to a decrease in $\chi_{\text{eff}}N$, with N being the total block copolymer length. This shifts $\chi_{\text{eff}}N$ vertically downward, while f remains constant as shown in Figure 4, inducing the hexagonally packed $C\perp$ cylinders to the disordered state (1 \rightarrow 2). In the drying process of the swollen film, the χ_{eff} (or $\chi_{\text{eff}}N$) increases such that, the disordered structure re-transforms into cylinders (2 \rightarrow 3) rapidly within a few seconds. Since the silicon substrate used in this study is hydrophilic, P4VP chains, which have a strong affinity for Si, preferentially adsorb onto the silicon, while PS preferentially migrates at the air/polymer interface because of its low surface energy.^{61,62} Consequently, P4VP domains with the substrate favours the formation of parallel cylinders. The GISAXS image shows two reflections in the Yoneda band, but do not show any Bragg rods with vertical streaks that are characteristic of the $C\perp$ cylinders. It is worth mentioning here that no ring like features are observed in the GISAXS 2D pattern in the dried sample, which are characteristic feature of random orientation of parallel cylinders.⁶³ These results suggest that the parallel cylinders are well ordered at least in the length scale comparable to the coherent length of X-rays ($\sim 1 \mu\text{m}$). As shown in Fig. 1, the SFM image validate the presence of such large grains composed of the parallel cylinders in the dried state.

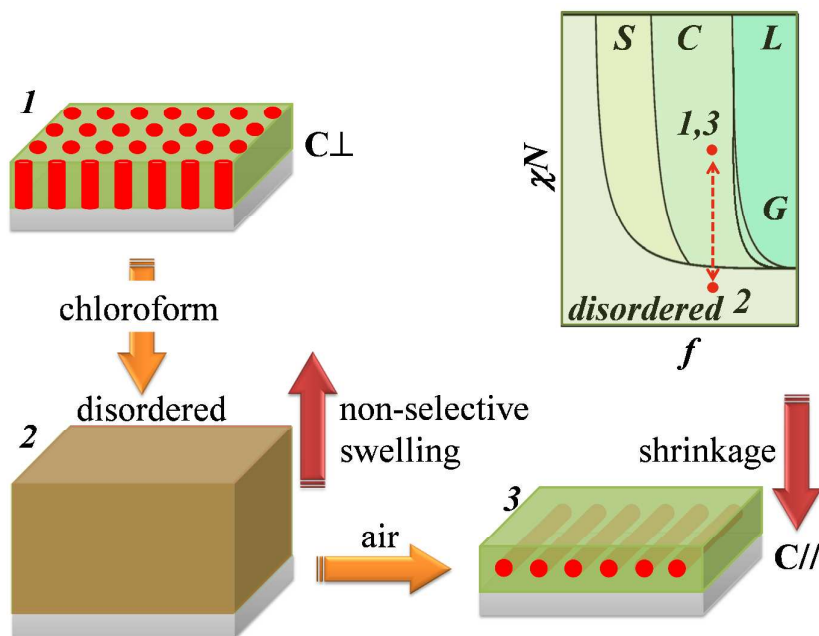


Figure 4. Schematic representation of microdomain re-orientation during swelling of block copolymer thin film in non-selective solvent (chloroform) vapors. Right top part of the diagram shows χN vs f .

Solvent vapor annealing of perpendicular cylinders (C⊥) in the selective solvent (1,4-dioxane):

In this section, we discuss the structural changes upon solvent vapor annealing of the C⊥ in the selective solvent (i.e., 1,4-dioxane) for PS, which is a majority component of the PS-*b*-P4VP block copolymer used in this work. Figure 5 shows sequences of GISAXS images at different intervals of time during the swelling under 1,4-dioxane vapors. In this experiment the starting GISAXS image (at $t=0$) shows sharp Bragg rods up to fourth order whose ratios of the peak positions relative to the first order peak position are assigned to be 2:3:4. Upon exposure to 1,4-dioxane vapors, in contrast to the previous case, the Bragg rods remain intact even in the swollen state.

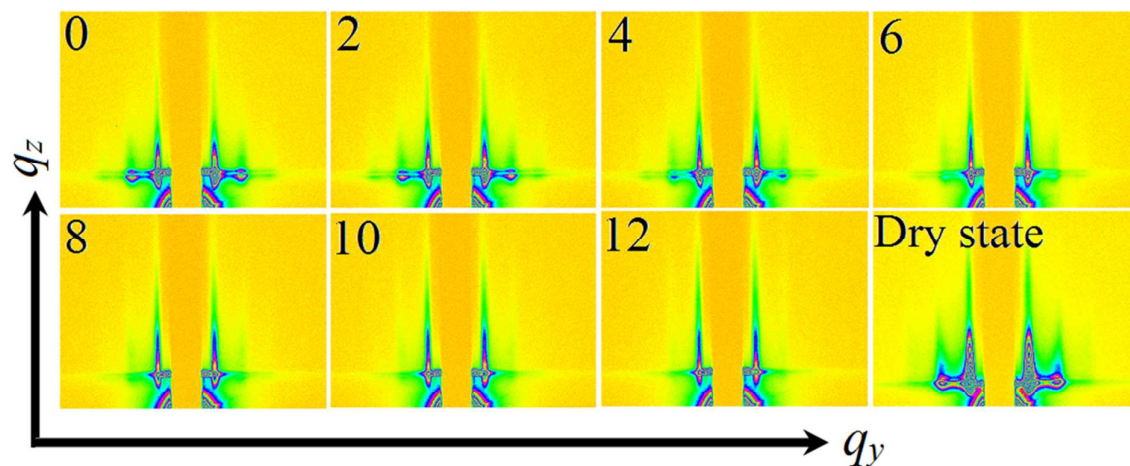


Figure 5. Time-resolved GISAXS images collected for C_{\perp} oriented PS-b-P4VP cylinders upon exposure to the saturated vapors of 1,4-dioxane. The last image was collected after surface reconstruction of the dried film in ethanol. Numbers on each image represents 1,4-dioxane vapor exposure time in minutes. Data are from Ref. 41.

No changes in the peak positions of the Bragg rods were observed upon the 1,4-dioxane vapor annealing. The variation in the intensity maxima of the first and second order peaks of the *in-plane* GISAXS (intensity vs q_y) are plotted against time in Figure 6. From the figure we can see that the intensity of the first order peak slightly increases with the annealing time, whereas the intensity of the second order peak decreases marginally with increasing the solvent vapor annealing time. This observation is very different from the previous case, where the intensities of the Bragg rods were drastically reduced with the chloroform vapor annealing time, suggesting that the swollen state remains microphase separated in the case of the selective solvent. After evaporation of the solvent, the 2D GISAXS pattern shown in Figure 5 remains almost unchanged indicating the cylinders oriented perpendicular to the surface persists.

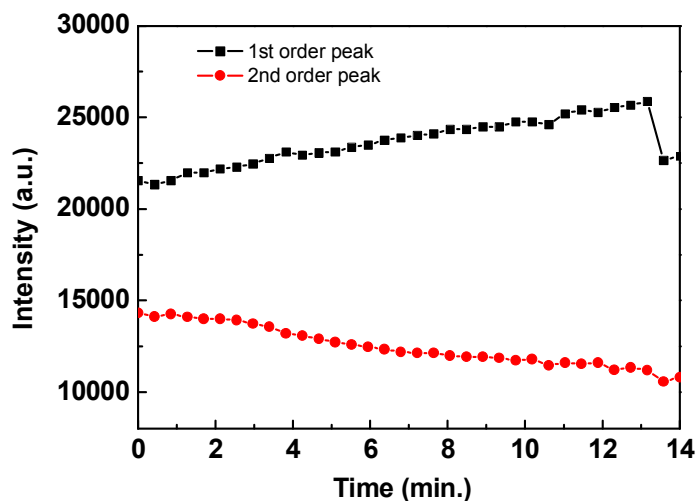


Figure 6. Time-resolved *in-plane* GISAXS intensity maximum of 1st and 2nd order scattering peaks evaluated from *in-plane* GISAXS line profiles collected for the perpendicularly oriented PS-*b*-P4VP cylinders ($C\perp$) upon exposure to saturated 1,4-dioxane vapors.

In order to understand the changes in the internal structures of the block copolymer thin film upon swelling, *out-of-plane* GISAXS (intensity vs q_z) line profiles at $q_y = 0.22 \text{ nm}^{-1}$ extracted from the 2D GISAXS images are shown in Figure 7. With the progress of 1,4-dioxane vapor annealing time, obvious changes in the swollen state are observed in the *out-of-plane* GISAXS line profiles: At $t=0$, no peaks were observed, but after 6 min., a broad peak appeared at around $q_z = 0.24 \text{ nm}^{-1}$ and its intensity increased with time up to 14 min, as indicated with the arrow in Figure 7. The appearance of the *out-of-plane* Bragg reflections in the swollen state is attributed to the formation of a microphase separated structure within the film. After solvent removal, this broad peak almost disappeared and the line profile matches with the profile at $t=0$, which is typical for the $C\perp$ cylinders. We postulate that the appearance and disappearance of the peak at $q_z = 0.24 \text{ nm}^{-1}$ represents the order-order transition of the PS-*b*-P4VP thin film from cylinders to discrete objects (spheres or ellipsoids, as will be discussed below) in presence of selective solvent vapors.

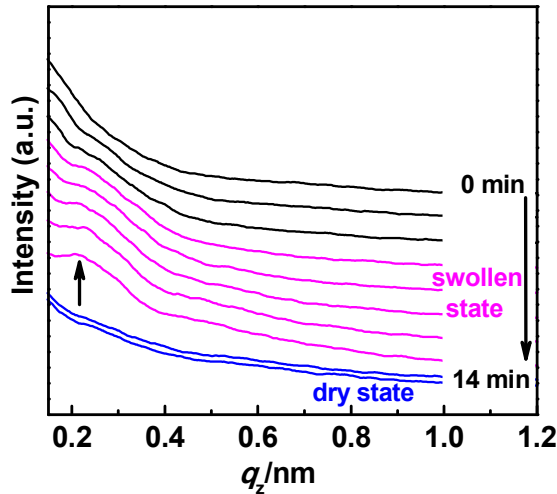


Figure 7. Time dependence of the *out-of-plane* GISAXS line profiles at $q_y = 0.22 \text{ nm}^{-1}$ extracted from Figure 5. Each data from top corresponds to 1.5 min time interval from $t=0$ min.

In order to provide insight into the transient structure via the order-order transition, the *out-of-plane* GISAXS line profile for the swollen film in 1,4-dioxane vapors was analysed in detail. Figure 8 shows the *out-of-plane* line profile where we can see the broad (roll-over) peak at around $q_z = 0.45 \text{ nm}^{-1}$ along with the first-order scattering maximum at $q_z = 0.24 \text{ nm}^{-1}$ after 12 min. It is reasonable to assume that the first order peak is attributed to the lattice factor, while the roll-over region corresponds to the form factor of the discrete object. For this purpose, we employed a paracrystal theory. The paracrystal analysis compared the experimental scattering profile with the calculated one with a body-centered-cubic lattice with paracrystal distortion.^{64,65} Here we also considered the polydispersity of R given by a Gaussian function:

$$P(R) \sim \exp[-(R - \bar{R})^2 / 2\sigma^2] \quad (2)$$

Where \bar{R} and σ are the average R and corresponding standard deviation, respectively. However, as shown in Figure 8, we found that the best-fitted scattering profile for the

spherical model with $\bar{R} = 1.5$ nm and $\sigma = 0.5$ nm (the red solid line) by using the paracrystal theory could satisfy only the experimental profile (open circles) up to $q \cong 0.07$ nm⁻¹. Also it is clear that the calculated scattering profile near the first order peak (with the interdomain spacing of 35 nm and the lattice distortion factor (or so-called g-factor) of 0.2) is quite different from the experimental profile. It should be noted that these parameters indicate that the transient lattice order is less compact and quite distorted, making the accuracy of the data fitting somewhat ambiguous. Here we do not discuss the lattice order further.

Taking the deviation from the spherical model at $0.07 < q < 0.1$ nm⁻¹ into account, we then assumed that the shape of the transient microdomain unit was ellipsoidal. In fact, Russell and co-workers reported the mechanism of microdomain re-orientation from parallel cylinders to perpendicular cylinders in presence of electric field.⁶⁶ The fluctuations caused by the applied electric field break up the parallel cylindrical microdomains into spherical microdomains, and these spherical microdomains then deformed into ellipsoidal domains that reconnected into cylindrical microdomains. Motivated by their results, we assumed that the broad rollover peak is attributed to the form factor of ellipsoids as a result of a transient structure of cylinders in the solvent. The scattering intensity from an ellipsoid of revolution (R_d, R_d, wR_d) with a random orientation is given as follows:

$$F(q) = \int_0^\pi (4\pi w R_d^3 / 3)^2 \Phi^2(u) \sin \beta d\beta \quad (3)$$

where

$$\Phi(u) = \frac{3}{u^3} (\sin u - u \cos u) \quad (4)$$

with

$$u = q R_d [\sin^2 \beta + w^2 \cos^2 \beta]^{1/2} \quad (5)$$

and R_d , w and β are radius of ellipsoid, an aspect ratio of the ellipsoid, and a polar angle between the axis of revolution and the reference axis, respectively. As shown in Figure 10,

the ellipsoidal model (the solid line) with $R_d = 2.0 \pm 0.2$ nm and $w = 2.6 \pm 0.3$ shows a reasonable fit to the data up to $q = 1$ nm⁻¹. Hence, we can see that the radius of the ellipsoids decreases by about 50% compared to the original cylinders. This can be explained by the fact that, the elongated (swollen) P4VP cylindrical microdomains in the direction normal to the film surface with the solvent should be contracted in the direction parallel to the film surface, in order to conserve the mass of the polymer (since P4VP does not dissolve in 1,4-dioxane).^{67,68}.

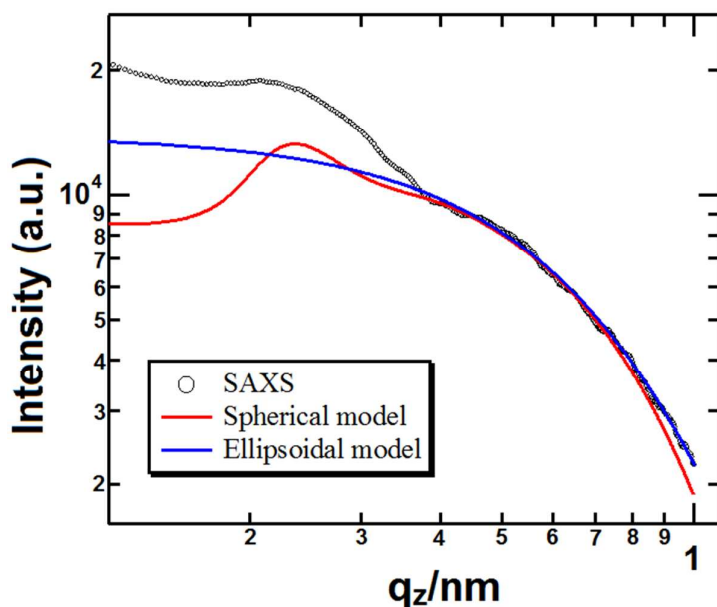


Figure 8. *Out-of-plane* GISAXS line profile extracted for the swollen film in 1,4-dioxane vapors after 12 min. Circles: Experimental data; Red line: Calculated scattering profile for the spherical model with $R = 1.5$ nm, $\sigma = 0.5$ nm, interdomain spacing of 35 nm, the g-factor of 0.2 by using the paracrystal theory; Blue line: best-fit to the data on the basis of the ellipsoidal model by using eqs (3)-(5) with $R_d = 2$ nm and $w = 2.6$.

Figure 9 shows a schematic model for the microdomain re-orientation upon swelling in a selective solvent (1,4-dioxane) and the effect can be discussed in conjunction with the phase diagram χN vs f . 1,4-Dioxane is a good solvent for the majority block PS, but a poor solvent

for the minority block P4VP. The effect of a selective solvent is more complicated in diblock copolymer systems because both f and χ_{eff} change. There are intensive reports on order-order transitions in block copolymer systems in presence of selective solvents,^{39,69,70} or homopolymers,^{71,72} variation of temperature,^{67,68,73} and the application of external fields, such as electric fields, magnetic fields, and shear flow.⁷⁴⁻⁷⁶ When the PS-*b*-P4VP is swollen by a selective solvent, the χ_{eff} (eq 1) value increases when the absolute value of the difference between PS/1,4-dioxane and P4VP/1,4-dioxane interaction parameters ($\Delta\chi$) is higher than 0 and/or the volume fraction of the copolymer in 1,4-dioxane (ϕ) decreases. For large swelling, ϕ will dominate, resulting in a decrease in χ_{eff} again.⁶⁰ At the same time, 1,4-dioxane has an affinity for PS blocks and changes the volume ratio of the two copolymer blocks.

In the present work, as a result of selective swelling of the PS matrix, the cylindrical microdomains of P4VP deform into the ellipsoidal domains in the swollen state without transition to the disordered state. From the previous scattering study, it was found that the Flory-Huggins interaction parameter lies between $0.317 < \chi_{\text{PS-P4VP}} < 0.347$ (temperature between 160 and 195 °C) for the PS-*b*-P4VP diblock copolymer.⁷⁷ Such a large χ value suggests that PS-*b*-P4VP swells in vapors of a selective solvent without disordering. In the present case, the preferential swelling of the PS-*b*-P4VP thin films results in the order-order transition (OOT) (1→2) from cylindrical to ellipsoidal domain morphology in the vicinity of the sphere-cylinder phase boundary. Fast drying of the films leads to shrinkage of the microdomain structures in the direction along the film normal. Upon shrinkage, the solvent vapor should escape along the film normal, which could enhance the coalescence of the ellipsoidal domains along the film normal and which introduces anisotropy to the system. The escape rate of the solvent vapor is the main driving force for the fusion of the ellipsoidal domains. Ober and coworkers observed such a transition from cylindrical to spherical morphology upon annealing poly(α -methylstyrene)-*b*-poly(4-hydroxystyrene) thin films in a

selective solvent.⁴⁸ In that case, the spherical morphology was trapped kinetically in the dried state, possibly due to the rapid evaporation of solvent (acetone) used. But in the present work, upon the film shrinkage the ellipsoidal domains are approaching in the direction along the film normal and, finally, coalesce into perpendicular aligned cylinders ($2 \rightarrow 1$), which is kinetically preferable. In this way, we found that the selectivity of the solvent to constituting blocks and the solvent evaporation rate are mainly responsible for a particular kinetic pathway in the phase diagram and for the different alignments of the cylindrical microdomains in the PS-*b*-P4VP thin films.

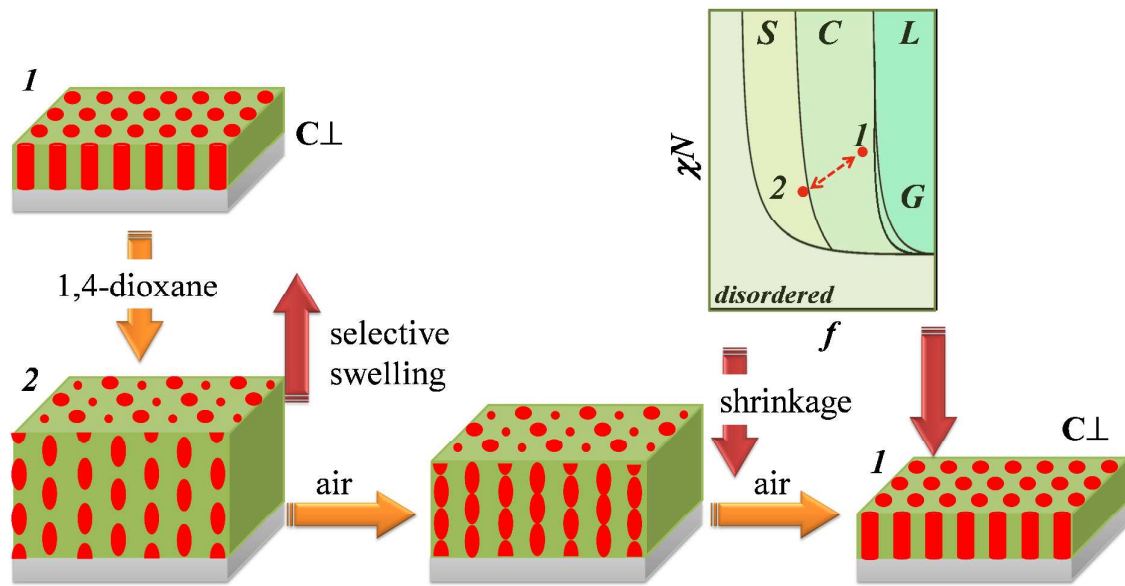


Figure 9. Schematic representation of structural changes upon swelling of PS-*b*-P4VP block copolymer thin film in the selective solvent (1,4-dioxane) vapors. Right top part of the diagram shows χN vs f . Swelling in the selective solvent drives the system on the route $1 \rightarrow 2$, resulting in the ellipsoidal morphology. Drying of the swollen film leads to the hexagonally packed perpendicular cylinders via $2 \rightarrow 1$.

Conclusions

By using the time-resolved in situ GISAXS and ex-situ scanning force microscopy, we have successfully clarified the novel pathways that control the orientations of cylindrical microdomains formed in PS-*b*-P4VP thin films upon annealing in different solvent vapors. The selectivity of the solvent to constituting blocks together with the geometry of drying determines the orientation of the cylindrical microdomains with respect to the substrate plane. Preferential swelling of the PS matrix in vapour of the selective solvent (1,4-dioxane) induces a morphological transition from cylindrical to ellipsoidal as a transient structure to spherical microdomains; subsequent solvent evaporation resulted in shrinkage of the matrix in the vertical direction, merging the ellipsoidal domains into the perpendicularly aligned cylinders. On the other hand, the swelling of the P4VP perpendicular cylinders ($C\perp$) in chloroform, a non-selective solvent vapors leads to the reorientation to in-plane cylinders through a disordered state.

Acknowledgements

EBG thanks Dr. Suresh Das for his constant support and encouragement. EBG also thanks Department of Science and Technology (Government of India) for the award of Ramanujan fellowship, IUSSTF and Alexander von Humboldt foundation for awarding research fellowships. EBG acknowledge the financial support from Council of Scientific and Industrial Research, Government of India under network project CSC-0114. We acknowledge the ESRF for provision of synchrotron radiation facilities and we would like to thank Dr. O. Konovalov and Dr. F. Zontone for assistance in using beam line ID10B. We also would like to thank Dr. B. Nandan and Dr. Marcus Böhme for their help during GISAXS measurements.

Associated Content:

Supporting Information Available: Figure S1: 2D GISAXS image collected for the perpendicularly oriented PS-b-P4VP cylinders ($C\perp$) at a rotation angle. Figure S2: *The* Out-of-plane GISAXS line profile at $t = 10$ min (swollen state) for perpendicularly oriented PS-b-P4VP cylinders ($C\perp$) upon the exposure to the saturated vapors of chloroform.

References

1. F.S. Bates, G.H. Fredrickson, *Annu. Rev. Phys. Chem.*, 1990, **41**, 525-557.
2. I.W. Hamely, *The physics of block copolymers*. Oxford University Press: New York, 1998.
3. S. B. Darling, *Prog. Polym. Sci.*, 2007, **32**, 1152-1204.
4. Fasolka, M.J.; Mayes, A.M., *Annu. Rev. Mater. Res.*, 2001, **31**, 323-355.
5. M. Muthukumar, C. K. Ober, E. L. Thomas, *Science*, 1997, **277**, 1225-1232.
6. F. S. Bates, G. H. Fredrickson, *Phys. Today*, 1999, **52**, 32-38.
7. A.-V. Ruzette, L. Leibler, *Nature Mater.*, 2005, **4**, 19-31.
8. T. P. Lodge, *Macromol. Chem. Phys.*, 2003, **204**, 265-273.
9. S. J. Metz, M. H. V. Mulder, M. Wessling, *Macromolecules*, 2004, **37**, 4590-4597.
10. J. Rzaev, M. A. Hillmyer, *J. Am. Chem. Soc.*, 2005, **127**, 13373-13379.
11. T. Thurn-Albrecht, J. Schotter, G. A. Kastle, N. Emley, T. Shibauchi, L. Krusin-Elbaum, K. Guarini, C. T. Black, M. T. Tuominen, T. P. Russell, *Science*, 2000, **290**, 2126-2129.
12. M. J. Misner, H. Skaff, T. Emrick, T. P. Russell, *Adv. Mat.*, 2003, **15**, 221-224.
13. B. Nandan, E. B. Gowd, N. Bigall, A. Eychmüller, P. Formanek, P. Simon, M. Stamm, *Adv. Funct. Mater.*, 2009, **19**, 2805-2811.
14. E. B. Gowd, B. Nandan, N. C. Bigall, A. Eychmüller, P. Formanek, M. Stamm, *Polymer*, 2010, **51**, 2661-2667.

15. E. J. W. Crossland, M. Kamperman, M. Nedelcu, C. Ducati, U. Wiesner, D. M. Smilgies, G. E. S. Toombes, M. A. Hillmyer, S. Ludwigs, U. Steiner, H. J. Snaith, *Nano Lett.*, 2009, **9**, 2807-2812.
16. B. Lee, J. Yoon, W. Oh, Y. Hwang, K. Heo, K. S. Jin, J. Kim, K.-W. Kim, M. Ree, *Macromolecules*, 2005, **38**, 3395-3405.
17. S. Park, D. H. Lee, J. Xu, B. Kim, S. W. Hong, U. Jeong, T. Xu, T. P. Russell, *Science*, 2009, **323**(5917), 1030-1033.
18. I. W. Hamley, *Prog. Polym. Sci.*, 2009, **34**, 1161-1210.
19. J. N. L. Albert, T. H. Epps, III., *Mater. Today*, 2010, **13**, 24-33.
20. M. Luo, T. H. Epps, *Macromolecules*, 2013, **46**, 7567-7579.
21. K. Amundson, E. Helfand, D. D. Davis, E. Quan, S. S. Patel, S. D. Smith, *Macromolecules*, 1991, **24**, 6546-6548.
22. P. Mansky, J. DeRouchey, T. P. Russell, J. Mays, M. Pitsikalis, T. Morkved, H. Jaeger, *Macromolecules*, 1998, **31**, 4399-4401.
23. K. Schmidt, H. G. Schoberth, M. H. Z. Ruppel, H. Hänsel, T. M. Weiss, V. Urban, G. Krausch, A. Böker, *Nature Materials*, 2008, **7**, 142-145.
24. R. J. Albalak, E. L. Thomas, *J. Polym. Sci., Part B: Polym. Phys.*, 1994, **32**, 341-350.
25. S. O. Kim, H. H. Solak, M. P. Stoykovich, N. J. Ferrier, J. J. de Pablo, P. F. Nealey, *Nature*, 2003, **424**, 411-414.
26. R. Ruiz, H. Kang, F. A. Detcheverry, E. Dobisz, D. S. Kercher, T. R. Albrecher, J. J. de Pablo, P. F. Nealey, *Science*, 2008, **321**, 936-939.
27. C. De Rosa, C. Park, E. L. Thomas, B. Lotz, *Nature*, 2000, **405**, 433-437.
28. G. Reiter, G. Castelein, P. Hoerner, G. Riess, A. Blumen, J. U. Sommer, *Phys. Rev. Lett.*, 1999, **83**, 3844-3847.

29. A. Sidorenko, I. Tokarev, S. Minko, M. Stamm, *J. Am. Chem. Soc.*, 2003, **125**, 12211-12216.
30. B. Nandan, M. K. Vyas, M. Boehme, M. Stamm, *Macromolecules*, 2010, **43**, 2463-2473.
31. P. Busch, D. Posselt, D.-M. Smilgies, B. Rheinländer, F. Kremer, C. M. Papadakis, *Macromolecules*, 2003, **36**, 8717-8727.
32. A. Sepe, Z. Di, D. Posselt, D.-M. Smilgies, C. M. Papadakis, *J. Phys.: Cond. Matt.*, 2011, **23**, 254213.
33. P. Busch, D. Posselt, D.-M. Smilgies, M. Rauscher, C. M. Papadakis, *Macromolecules*, 2007, **40**, 630-640.
34. S. H. Kim, M. J. Misner, T. Xu, M. Kimura, T. P. Russell, *Adv. Mater.*, 2004, **16**, 226-231.
35. K. Fukunaga, H. Elbs, R. Magerle, G. Krausch, *Macromolecules*, 2000, **33**, 947-953.
36. R. J. Albalak, M. S. Capel, E. L. Thomas, *Polymer*, **1998**, *39*, 1647-1656.
37. Y. Xuan, J. Peng, L. Cui, H. F. Wang, B. Y. Li, Y. C. Han, *Macromolecules*, 2004, **37**, 7301-7307.
38. Z. Di, D. Posselt, D.-M. Smilgies, R. Li, M. Rauscher, I. I. Potemkin, C. M. Papadakis, *Macromolecules*, 2012, **45**, 5185-5195.
39. K. J. Hanley, T. P. Lodge, C. I. Huang, *Macromolecules*, 2000, **33**, 5918-5931.
40. K.A. Cavicchi, K.J. Berthiaume, T.P. Russell, *Polymer*, 2005, **46**, 11635-11639.
41. E. B. Gowd, M. Böhme, M. Stamm, *IOP Conf. Ser.: Mater. Sci. Eng.*, 2010, **14**, 012015.
42. E. B. Gowd, B. Nandan, M. K. Vyas, N. C. Bigall, A. Eychmüller, H. Schlörb, M. Stamm, *Nanotechnology*, 2009, **20**, 415302.

43. Z. Di, D. Posselt, D.-M. Smilgies, C. M. Papadakis, *Macromolecules*, 2010, **43**, 418-427.
44. C. Sinturel, M. Vayer, M. Morris, M. A. Hillmyer, *Macromolecules*, 2013, **46**, 5399-5415.
45. T.-Y. Lo, C.-C. Chao, R.-M. Ho, P. Georgopoulos, A. Avgeropoulos, E. L. Thomas, *Macromolecules*, 2013, **46**, 7513-7524.
46. K. A. Cavicchi, T. P. Russell, *Macromolecules*, 2007, **40**, 1181-1186.
47. J. K. Bosworth, M. Y. Paik, R. Ruiz, E. L. Schwartz, J. Q. Huang, A. W. Ko, D.-M. Smilgies, C. T. Black, C. K. Ober, *ACS Nano*, 2008, **2**, 1396-1402.
48. M. Y. Paik, J. K. Bosworht, D. M. Smilges, E. L. Schwartz, A. Xavier, C. K. Ober, *Macromolecules*, 2010, **43**, 4253-4260.
49. T. H. Kim, J. Huh, J. Hwang, H.-C. Kim, S. H. Kim, B.-H. Sohn, C. Park, *Macromolecules*, 2009, **42**, 6688-6697.
50. S. Park, B. Kim, J. Y. Wang, T. P. Russell, *Adv. Mater.*, 2008, **20**, 681-685.
51. S. Park, J. Y. Wang, B. Kim, J. Xu, T. P. Russell, *ACS Nano*, 2008, **2**, 766-772.
52. W. H. Huang, P. Y. Chen, S. H. Tung, *Macromolecules*, 2012, **45**, 1562-1569.
53. H. Tanaka, T. Hashimoto, *Polym. Commun.*, 1988, **29**, 212-216.
54. N. Sakamoto, T. Hashimoto, C. D. Han, D. Kim, N. Y. Vaidya, *Macromolecules*, 1997, **30**, 1621-1632.
55. N. Sakamoto, T. Hashimoto, C. D. Han, D. Kim, N. Y. Vaidya, *Macromolecules*, 1997, **30**, 5321-5330.
56. J. N. L. Albert, W.-S. Young, R. L. Lewis, T. D. Bogart, J. R. Smith, T. H. Epps, *ACS Nano*, 2012, **6**, 459-466.

57. D. W. van Krevelan, P. J. Hoftyzer, *Properties of Polymers: Their Estimation and Correlation Length with Chemical Structure*, 2nd ed.; Elsevier Scientific Publishing Co.: New York, 1976.
58. E. A. DiMarzio, J. H. Gibbs, *J. Polym. Sci., Part A*, 1963, **1**, 1417-1428.
59. T. S. Chow, *Macromolecules*, 1980, **13**, 362-364.
60. Y. Li, X. Wang, I. C. Sanchez, K. P. Johnston, P. F. Green, *J. Phys. Chem. B*, 2007, **111**, 16-25.
61. Y. Liu, W. Zhao, X. Zheng, A. King, A. Singh, M. H. Rafailovich, J. Sokolov, K. H. Dai, E. J. Kramer, S. A. Schwarz, O. Gebizlioglu, S. K. Sinha, *Macromolecules*, 1994, **27**, 4000-4010.
62. H. Yokoyama, T. E. Mates, E. J. Kramer, *Macromolecules*, 2000, **33**, 1888-1898.
63. B. Lee, W. Oh, Y. Hwang, Y.-H. Park, J. Yoon, K. S. Jin, K. Heo, J. Kim, K.-W. Kim, M. Ree, *Adv. Mater.*, 2005, **17**, 696-701.
64. H. Matsuoka, H. Tanaka, T. Hashimoto, N. Ise, *Phys. Rev.* 1987, **B36**, 1754.
65. H. Matsuoka, H. Tanaka, N. Iizuka, T. Hashimoto, N. Ise, *Phys. Rev.* 1990, **B41**, 3854.
66. T. Xu, A. V. Zvelindovsky, G. J. A. Sevink, K. S. Lyakhova, H. Jinnai, T. P. Russell, *Macromolecules*, 2005, **38**, 10788-10798.
67. K. Kimishima, K. Saijo, T. Koga, T. Hashimoto, *Macromolecules*, 2013, **46**, 9032-9044.
68. K. Kimishima, T. Koga, T. Hashimoto, *Macromolecules*, 2000, **33**, 968-977.
69. Y. S. Liu, M. H. Li, R. Bansil, M. Steinhart, *Macromolecules*, 2007, **40**, 9482-9490.
70. T. P. Lodge, B. Pudil, K. J. Hanley, *Macromolecules*, 2002, **35**, 4707-4717.
71. L. Gao, J. Yao, Z. Shen, Y. Wu, X. Chen, X. Fan, Q. Zhou, *Macromolecules*, 2009, **42**, 1047-1050.

72. Y.-Y. Huang, J.-Y. Hsu, H.-L. Chen, T. Hashimoto, *Macromolecules*, 2007, **40**, 3700-3707.
73. J. Yoon, S. Jin, B. Ahn, Y. Rho, T. Hirai, R. Maeda, T. Hayakawa, J. Kim, K. W. Kim, M. Ree, *Macromolecules*, 2008, **41**, 8778-8784.
74. D. Q. Ly, T. Honda, T. Kawakatsu, A. V. Zvelindovsky, *Macromolecules*, 2007, **40**, 2928-2935.
75. K. Schmidt, H. G. Schoberth, M. Ruppel, H. Zettl, H. Hansel, T. M. Weiss, V. Urban, G. Krausch, A. Boker, *Nature Mater.*, 2008, **7**, 142-145.
76. Y.-R. Hong, D. H. Adamson, P. M. Chaikin, R. A. Register, *Soft Matter*, 2009, **5**, 1687-1691.
77. W. Zha, C. D. Han, D. H. Lee, S. H. Han, J. K. Kim, J. H. Kang, C. Park, *Macromolecules*, 2007, **40**, 2109-2119.